Temporal compositional variation of syn-rift rhyolites along the western margin of the southern Red Sea and northern Main Ethiopian Rift

D. AYALEW[1], C. EBINGER[2], E. BOURDON[2,3], E. WOLFENDEN[2], G. YIRGU[1] & N. GRASSINEAU[2]

[1]*Department of Earth Sciences, Addis Ababa University, PO Box 729/1033 Addis Ababa, Ethiopia (e-mail: dereayal@geol.aau.edu.et)*

[2]*Department of Geology, Royal Holloway University of London, Egham, TW20 0EX, UK*

[3]*Now at: Institut de Geologie, Université de Neuchatel, Rue Emile Argand 11, CP 2, 2007 Neuchatel, Switzerland*

Abstract: Structural and geochronological relations indicate that the felsic rocks at the top of the Oligocene flood basalt sequences in the Afar volcanic province were erupted coevally with the initial rifting in the Red Sea and Gulf of Aden. In this study, we use the newly established volcanic–tectonic history to examine the geochemical evolution with time of felsic volcanics as rifting has progressed to seafloor spreading in the southern Red Sea and northern Main Ethiopian Rift. Geochemical analyses (major and trace elements; Sr, Nd and O isotopic compositions) of syn-rift rhyolites ranging in age from 28 to 2.5 Ma indicate that the rhyolites can be derived from mantle-sourced basaltic magma through fractional crystallization accompanied by variable amounts of crustal contamination (e.g. $^{87}Sr/^{86}Sr = 0.70489–0.70651$; $^{143}Nd/^{144}Nd = 0.51254–0.51283$; $\delta^{18}O = +4.5$ to $+6.4‰$). The input of crust tends to increase with time, which suggests the weakening and heating of the crust in response to lithospheric thinning and magma injection in the past *c.* 30 Ma. These results support earlier structural and thermomechanical models for rift formation in the southern Red Sea rift and the younger, less-evolved northern Main Ethiopian Rift system.

The initiation of continental flood basalt (CFB) magmatism is spatially and temporally related to continental break-up, which results in the formation of oceanic crust, at least within the past 200 Ma. However, the relationships between the timing of CFB formation and rifting leading to ocean-floor formation are complex, and can vary in time and space (see also Courtillot *et al.* 1999; Hawkesworth *et al.* 1999; Menzies *et al.* 2002). Magmatism can predate continental extension by several million years (e.g. Ethiopia–Yemen), magmatism and break-up can be synchronous (e.g. Paraná–Etendeka, North Atlantic Tertiary volcanic province/Greenland–UK), or magmatism can postdate break-up by several million years (e.g. Australia–India). This is not unusual, in that plumes may interact with continental lithosphere independent of plate-driving forces. Although the details of plume melting remain controversial, there is agreement that lithospheric thinning or pre-existing thin zones are needed to produce the huge volumes of melt seen in CFB provinces.

In Ethiopia, Oligocene–Miocene felsic volcanic strata (rhyolites and minor trachytes) capping the flood basalt sequences are well exposed along the western margin of the southernmost sector of the southern Red Sea and the northernmost Main Ethiopian Rift (MER). The rhyolites are preferentially localized on or near the border fault, indicating that rifting preceded or at least was coeval with the felsic volcanism in both the southern Red Sea rift and the northernmost Main Ethiopian Rift (Wolfenden *et al.* 2004, 2005). This shows a clear relationship between the emplacement of large volumes of rhyolite and formation of the large offset border fault systems. The timespan for silicic volcanism shows southward younging along the border fault and the silicic volcanism migrates from the wider border faults towards narrow (*c.* 10 km-wide) magmatic segments within the rift (Wolfenden *et al.* 2005). The overall observations show multiple episodes of riftward migration of the locus of magmatism and faulting through time.

Samples of felsic volcanic rock (pyroclastic flow and lava) from the western margin (Fig. 1) of the southern Red Sea and northern Main Ethiopian Rift, where precise geochronological data are available, were analysed for chemical (major and trace elements) and isotopic (Sr, Nd and O) determinations. Geochemical studies on precisely dated

From: YIRGU, G., EBINGER, C.J. & MAGUIRE, P.K.H. (eds) 2006. *The Afar Volcanic Province within the East African Rift System*. Geological Society, London, Special Publications, **259**, 121–130.
0305-8719/06/$15.00

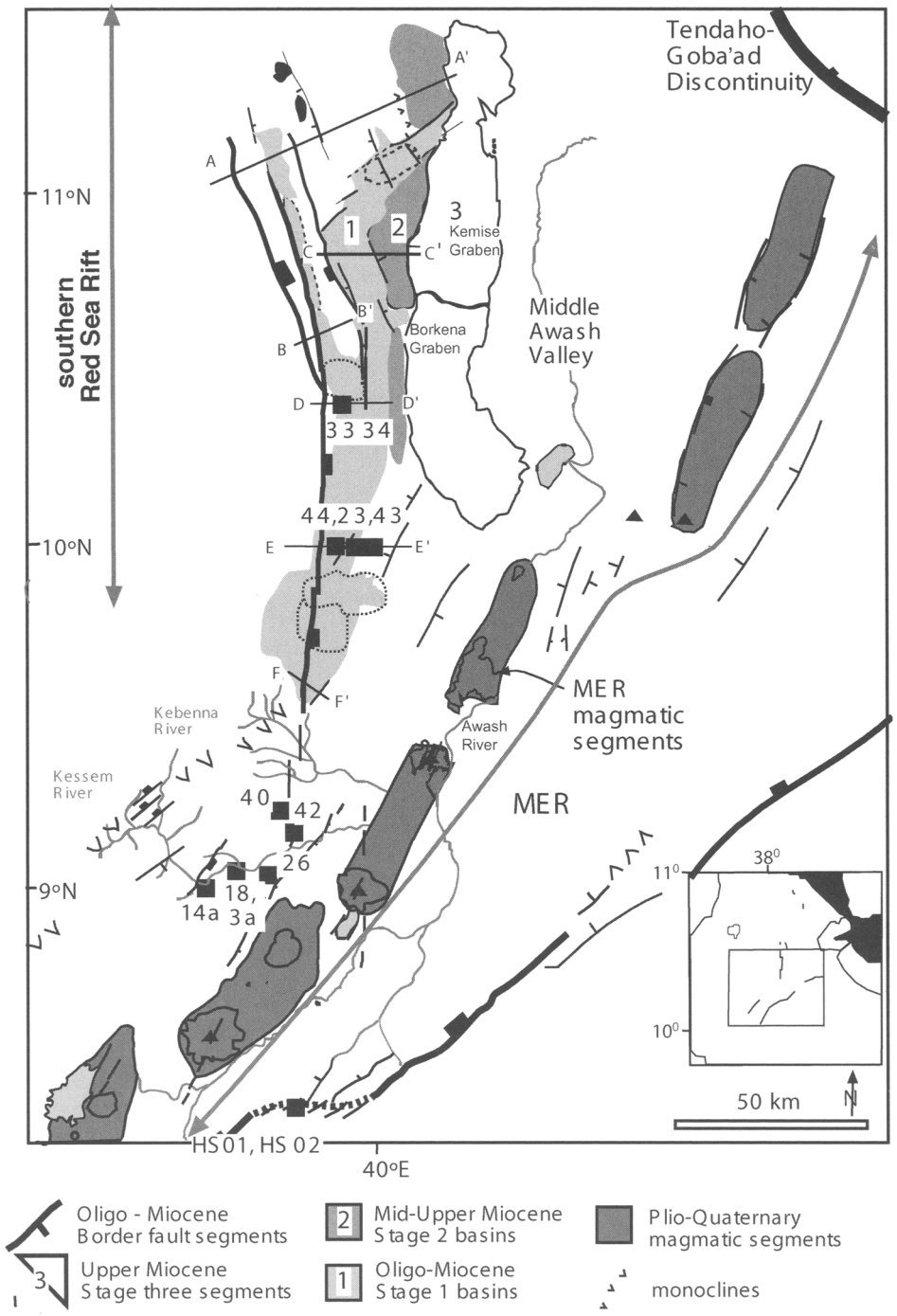

Fig. 1. Stages of basin development in the southernmost sector of the southern Red Sea and in the northern Main Ethiopian Rift (MER). BF = border fault. Numbering refers to stages of basin development in the Kemise, Ataye, Baso-Werena and Adama basins. The thin dashed lines enclose inter-basin volcanic complexes. Filled squares represent sample locations. The inset map shows the position of the study area with respect to the Red Sea–Afar–Main Ethiopian Rift triple junction. Adapted from Wolfenden *et al.* 2005.

samples are very sparse for the Ethiopian igneous province and this is the first comprehensive study. The main objective of this research is to constrain the geochemical evolution of the silicic volcanic rocks, which mark the onset of rifting in the southern Red Sea, through time in the light of existing and new data. We interpret our results in the light of new geophysical observations for the northern MER and uplifted plateau region that demonstrate significant modification of the crust and mantle lithosphere by magmatic processes (e.g. Kendall *et al.* 2005; Keranen *et al.* 2004; Mackenzie *et al.* 2005).

Tectonic setting

The Red Sea–Aden–Main Ethiopian Rift triple junction lies on the broad Ethiopian plateau, believed to have developed above a Palaeogene mantle plume (Marty *et al.* 1996; Pik *et al.* 1999; Schilling & Kingsley 1992). Compilations of $^{40}Ar/^{39}Ar$ data show that flood basalts and associated rhyolites were erupted across a *c.*1000 km diameter region between 31 and 29 Ma (Ayalew *et al.* 2002; Ayalew & Yirgu 2003; Baker *et al.* 1996; Coulié *et al.* 2003; Hofmann *et al.* 1997; Rochette *et al.* 1998; Ukstins *et al.* 2002), roughly coeval with the initiation of NE-directed extension in the southern Red Sea (Wolfenden *et al.* 2005) and the Gulf of Aden (Watchorn *et al.* 1998). An enigmatic province in southwestern Ethiopia comprising *c.* 1 km of basalts capped by rhyolites dated at 45 Ma may signal initial plume–lithosphere interactions (e.g. Ebinger *et al.* 1993; Ebinger & Sleep 1998) or mark a separate plume province (e.g. George *et al.* 1998).

Wolfenden *et al.* (2005) integrate geochronological data (Ukstins *et al.* 2002) and structural data, and show that rift formation had commenced by 29 Ma in the southern Red Sea rift, with faulting and basin subsidence propagating southward to *c.* 10° N. The Gulf of Aden rift had also initiated by 30 Ma (e.g. d'Acremont *et al.* 2005). Thus, rifting was coeval with the rhyolitic volcanism at the close of the flood basalt cycle. Initial rifting in the third arm of the Afar triple junction, the northernmost Main Ethiopian Rift (MER), initiated around *c.* 11 Ma (Chernet *et al.* 1998; Wolfenden *et al.* 2004). Initial crustal extension within the southern and central MER commenced between 18 and 15 Ma (Ebinger *et al.* 2000; WoldeGabriel *et al.* 1990). Thus, the MER, the northernmost sector of the East African rift system, propagated northward from the *c.* 25 Ma Turkana rift, a region of anomalously thinned lithosphere first rifted during Mesozoic time. The Red Sea–Aden–Main Ethiopian Rift triple junction is, therefore, a relatively young feature, developed only during the past 11 Ma, or 20 million years after the flood volcanism.

Age of silicic volcanism along the western margin

Along the western rift margin of the Afar depression, the flood volcanic sequences overlie marine sedimentary strata deposited on a passive continental margin in Mesozoic time (Hunegnaw *et al.* 1998). The volcanic packages are up to 2000 m thick and comprise basaltic lava flows overlain by rhyolites such as ignimbrites, airfall tuffs and lavas with interbedded basalts. The flood volcanic stratigraphy commonly shows a repetitious basalt–rhyolite succession. Silicic volcanics commonly constitute up to 50% of the preserved volcanic thickness and lie towards the top of the flood volcanic sequences. The rhyolitic centres comprise massive glassy effusive volcanic rocks and phenocryst-rich crystalline intrusions, and form irregular to dome-shaped flows.

The first silicic ignimbrite in the western margin of the Afar depression was erupted at 30.2 Ma and bimodal basalt–rhyolite volcanism continued in parts of the broad flood basalt province until 10 Ma (Kieffer *et al.* 2004; Wolfenden *et al.* 2004). The ages of the silicic volcanic rocks outside the faulted rift valley range from about 30 Ma in the north of the province to 10.8 Ma at Mount Guna (Kieffer *et al.* 2004). Silicic volcanism occurred early during the main basaltic episode and continued to erupt with Quaternary volcanism occurring in the rift valleys and central plateau. The range of dates for the studied rhyolites is from 30.2 to 2.5 Ma (Fig. 2).

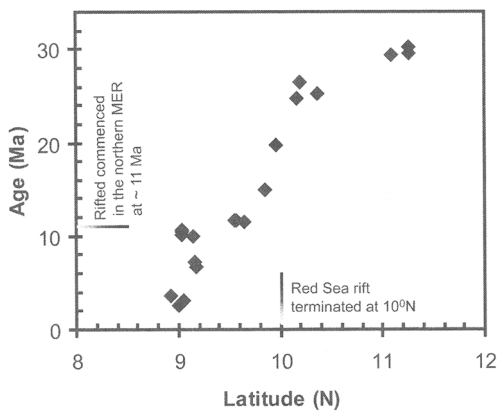

Fig. 2. Ages of silicic volcanic rocks in the western margin of the Afar depression, with migration of the centre of eruption from north to south. Note the Red Sea rift terminated at 10° N until linkage of the MER and southern Red Sea occurred at ~11 Ma.

Petrological characters of the silicic volcanic rocks

The Ethiopian volcanism (both plateau and rift) is bimodal with respect to SiO_2 content (basic–acidic distribution), a feature shared with most CFB. Intermediate rocks are scarce or absent. In the total alkalis–silica (TAS) classification, the volcanic rocks range from basalt, through basaltic andesite, trachybasalt, basaltic trachyandesite to trachyte and rhyolite (Ayalew *et al.* 2002; Kieffer *et al.* 2004; Peccerillo *et al.* 2003; Pik *et al.* 1998).

The silicic extrusive rocks are dominantly pyroclastic flows (welded and non-welded ignimbrites) with some lava that comprise phenocrysts (with up to 20 vol.% mode) and microphenocrysts largely of sanidine and quartz with minor amounts of opaques and clinopyroxene. The phenocrysts sometimes tend to occur in cumulophyric clots and are often broken and partially resorbed. The groundmass is commonly glassy showing eutaxitic texture and it is partially devitrified with dark brown stains and shows microcrystalline felsitic and spherulitic textures. The felsic rocks show evidence of hydrothermal alteration with surface colours of orange, pink, yellow, brown and red.

Silicic volcanic rocks consist mainly of rhyolite and minor trachyte (Table 1) and show mildly peralkaline affinity. There is one intermediate rock (Sample E01–3a). Sample E01–26 has anomalously high CaO (24%) and LOI (18%). For clarity, we simply refer to these rocks as rhyolites. The petrogenesis of the silicic volcanic rocks, including sample localities, petrography, stratigraphy, age and tectonic evolution, was presented in detail elsewhere (Ayalew *et al.* 2002; Ayalew & Yirgu 2003; Wolfenden *et al.* 2004, 2005) and are omitted from the forthcoming discussion. The geochemical character of the silicic rocks varies from north to south and within each region the character of the silicic rocks matches that of the underlying flood basalts.

Sr–Nd–O isotopes

Table 2 reports the Sr–Nd–O isotopic compositions of the rhyolites and an intermediate lava (sample E01–3a) along the western margin. The studied rhyolites have low Sr (<76 ppm, except sample E01–3a with Sr = 272 ppm) and high Rb (97–169 ppm) concentrations; consequently, they have high Rb/Sr ratios (1–11). The high Rb/Sr ratios are susceptible to even slight modification/alteration. The feldspar separates, on the other hand, have relatively low Rb/Sr ratios compared to the whole rock, so that their Sr isotopic compositions are more reliable than whole rock data. For this reason, Sr isotopic compositions of rhyolites were carried out on feldspar separates and the measured $^{87}Sr/^{86}Sr$ ratios are corrected to initial Sr isotope ratios. Alkali feldspars separated from the whole rocks have $^{87}Sr/^{86}Sr$ ratios that are markedly lower than their hosts (Table 2). Given the low Sm/Nd ratios of the studied rhyolites, the measured $^{143}Nd/^{144}Nd$ ratios are essentially considered to be the same as the initial $^{143}Nd/^{144}Nd$ ratios.

Figure 3 illustrates the Sr–Nd isotopic compositions of the study rhyolites compared to that of the plateau (Oligo-Miocene) and rift (Quaternary) rhyolites. This comparison reveals that Oligocene rhyolites, erupted probably under thick and perhaps cool crust, have the most mantle-like Sr and Nd isotopic ratios. The marginal rhyolites display lower $^{143}Nd/^{144}Nd$ and higher $^{87}Sr/^{86}Sr$ ratios compared to the plateau Oligocene rhyolites. They generally plot in the field of syn-rift Miocene and Quaternary rhyolites, indicating the link between faulting/rifting and silicic magma formation.

The oxygen isotopic compositions ($\delta^{18}O$ values) measured on quartz and alkali feldspar separates of the rhyolites range from +4.1 to +6.4‰. There are three values around +5.5‰, but the three other values are quite scattered. These values are substantially lower for rhyolites relative to the average values of most silicic volcanic rocks constrained to be between +7 and +8‰ (Eiler 2001), and may reflect that meteoric fluid circulation under high temperature conditions produced the ^{18}O-depletion (Criss & Taylor 1986). Meteoric water involved more progressively in the superficial magma chamber probably due to tectonic deformations.

Origin of marginal rhyolites

The west marginal rhyolites of the Afar depression cannot be derived from partial melting of the local crust, as they have relatively low initial $^{87}Sr/^{86}Sr$ ratios ~0.70549 and high $^{143}Nd/^{144}Nd$ ~0.51272, on average. Most Precambrian Ethiopian crustal rocks have $^{143}Nd/^{144}Nd$ ratios lower than those observed in the studied rocks (Asrat *et al.* 2004; Teklay *et al.* 1998).

Silicic partial melts of juvenile basaltic underplates cannot be distinguished from that derived by differentiation of basaltic magmas on major element variations, because both processes involve crystal–liquid equilibria. One possibility to discriminate partial melting from fractional crystallization trends is the variation patterns of compatible vs. incompatible elements (Cameron *et al.* 1996; Halliday *et al.* 1991; Hanson 1989). Figure 4 shows the variation of Sr (compatible element) vs. Zr (incompatible element) for west marginal rhyolites,

Table 1. *Major (wt %) and trace (ppm) elements for selected rhyolites along the western margin of the Afar depression*

Sample	EO1-14A	EO1-26	E01-18	EO1-3A	E01-42	E01-40	EEW00-23	EEW00-43	EEW00-44	EEW02-21	EEW00-34	EEW00-33	HS-01	HS-02
Age (Ma)	3.555	2.54	10.144	10.56	10.008	6.619	20–26	~ 19	15–19	11.673	~25	20–25	7.807	7.98
Lat (°N)	8.921	9	9.029	9.039	9.138	9.178	9.927	9.964	10.001	10.690	10.331	10.356	8.34	8.35
Long (°E)	39.5501	39.6325	39.5675	39.5653	39.7253	39.5428	39.981	39.937	39.869	40.025	39.847	39.832	39.6729	39.6699
SiO_2	75.23	52.71	73.96	67.24	73.67	74.37	73.51	72.58	71.55	73.55	74.78	75.20	70.32	71.70
TiO_2	0.41	0.36	0.46	1.11	0.37	0.35	0.38	0.48	0.66	0.41	0.42	0.30	0.34	0.43
Al_2O_3	10.72	8.52	11.22	15.51	11.02	11.07	10.01	13.70	14.48	10.81	13.14	12.18	13.45	10.37
$Fe_2O_3^*$	4.99	4.89	3.73	5.19	4.42	4.45	5.49	2.92	1.95	5.22	1.50	2.34	4.72	7.72
MnO	0.12	0.19	0.08	0.15	0.09	0.10	0.18	0.03	0.08	0.17	0.04	0.05	0.11	0.27
MgO	0.22	0.38	0.14	2.08	0.03	0.21	0.22	0.39	0.35	0.13	0.06	0.12	0.11	0.08
CaO	0.41	24.28	0.29	2.17	0.13	0.29	0.30	0.52	0.37	0.25	0.32	0.19	0.35	0.47
Na_2O	4.13	2.79	4.59	2.48	4.08	2.45	4.65	1.11	5.05	4.63	4.21	3.67	5.08	3.65
K_2O	4.61	4.51	4.40	4.36	4.82	5.65	4.56	7.48	5.49	4.51	4.84	4.95	4.75	4.38
P_2O_5	0.04	0.14	0.05	0.22	0.04	0.03	0.04	0.03	0.07	0.03	0.04	0.02	0.03	0.03
Total	100.87	98.78	98.93	100.51	98.66	98.96	99.34	99.25	100.05	99.70	99.36	99.02	99.25	99.09
LOI	2.67	17.98	0.59	7.15	0.65	3.14	0.77	2.18	0.66	1.00	0.38	1.19	1.02	4.26
Ni	3.2	7.1	4.5	5.7	3.4	6.4	5.9	3.9	3.4	5.8	6.9	5.8	7.0	4.1
Cr	2.3	4.6	2.6	3.5	2.5	6.3	7.2	3.1	3.2	3.0	4.6	3.7	2.8	4.1
V	6.8	5.1	11.2	21.9	6.5	10.8	11.9	10.4	9.5	9.2	5.3	7.1	4.8	1.3
Sc	1.5	1.0	8.3	10.1	6.4	5.3	5.4	5.5	5.1	2.2	5.7	3.3	2.6	2.1
Zn	226.2	185.5	131.8	130.5	178.8	282.5	278.6	195.9	103.0	203.1	156.1	123.3	181.0	290.6
Ga	29.0	20.4	28.3	25.7	29.4	32.8	32.2	29.6	29.2	31.4	27.9	28.1	30.3	31.4
Pb	21.0	13.4	10.6	16.2	13.8	22.5	21.7	13.8	17.4	17.1	14.6	15.6	19.5	23.4
Sr	16.6	75.5	17.0	271.9	12.5	16.0	16.0	64.6	40.9	10.7	72.0	35.1	14.5	22.0
Rb	168.6	96.7	107.4	81.2	121.3	150.3	160.6	140.4	130.3	120.1	128.4	150.0	166.5	145.1
Ba	90.8	306.1	331.8	817.2	247.3	49.2	67.0	417.3	432.5	80.7	579.2	305.5	145.3	304.0
Zr	957.2	855.5	863.3	663.8	1181.8	1736.2	1564.2	982.9	1035.7	906.4	737.9	696.4	1404.8	1152.3
Nb	118.8	116.0	108.1	74.3	137.4	197.2	168.7	120.5	166.4	105.8	111.5	125.7	151.7	159.1
Th	20.0	12.8	15.5	11.8	17.4	23.1	28.0	14.1	23.1	13.9	17.0	20.3	19.0	18.4
Y	118.7	103.8	69.4	72.0	88.8	200.0	159.7	97.4	86.1	101.5	92.0	74.3	110.3	127.9
La	129.8	91.6	82.7	91.3	83.8	156.2	190.8	112.2	130.6	85.3	141.8	88.9	102.6	148.5
Ce	220.6	179.2	166.8	189.4	178.6	294.0	349.4	226.4	252.9	204.0	155.0	147.1	207.6	276.6
Nd	116.2	83.4	78.8	87.6	81.2	168.6	169.6	100.4	99.0	84.7	130.6	86.0	78.5	122.4

The data are presented in geographical order. Sample E01–26 has anomalously high CaO (24%) and LOI (18%). Age data are from Ukstins *et al.* (2002); Wolfenden *et al.* (2004, 2005).
*Total Fe was analysed as Fe_2O_3

Table 2. *Sr–Nd–O isotopic compositions of rhyolites from along the western margin of Afar depression*

Sample	Age (Ma)	Phase	$^{87}Sr/^{86}Sr$	$^{87}Sr/^{86}Sr_i$	$^{143}Nd/^{144}Nd$	Qz/AF$\delta^{18}O$ (‰)
E 01–3a	10.56	WR	0.705537 ± 10	0.705411	0.512654 ± 5	
		AF	0.705445 ± 10	0.705363		
E 01–14a	3.56	WR			0.512569 ± 6	
E-01–26	2.54	WR			0.512778 ± 5	+5.69
E 01–18	10.14	WR			0.512797 ± 6	
		WR			0.512794 ± 4	
					mean 0.512796	
		AF	0.704893 ± 16	0.704814		
E 01–40	6.62	WR			0.512815 ± 4	+4.56
		AF	0.706508 ± 10	0.706429		
E 01–42	10.01	WR			0.512834 ± 5	
		WR			0.512826 ± 4	
		WR			0.512834 ± 4	
					mean 0.512831	
EEW 02–21	11.67	WR			0.512658 ± 4	+6.36
		WR			0.512652 ± 5	
					mean 0.512655	
EEW 00–23	19.76	WR			0.512762 ± 4	+4.69
EEW 00–33	25.52	WR	0.708968 ± 10	0.704594	0.512768 ± 5	
		AF	0.705355 ± 9	0.705156		
EEW 00–34	25.52	WR	0.706879 ± 12	0.705054	0.512769 ± 4	+5.57
		AF	0.705275 ± 10	0.705076		
EEW 00–43	19.76	AF	0.70579 ± 10	0.705636		+5.37
EEW00–44	19.76	WR	0.708496 ± 12	0.705971	0.512720 ± 4	
HS01	7.81	WR			0.512538 ± 5	
HS02	7.98	WR			0.512708 ± 5	

WR, whole rock; AF, alkali feldspar; Qz, quartz.

Sr and Nd isotope ratios were determined on the VG354 Thermal Ionization Spectrometer at Royal Holloway University of London using multidynamic techniques procedures and normalization described in Thirlwall (1991a and b). For Nd, powder samples were leached for 1 h in hot 6 M HCl. For Sr on alkali feldspar, crystals were handpicked to eliminate oxidation and glass or matrix, and leached for 1/2 h in hot 2.5 M HCl. In both case, leachate was removed by multiple rising in ultra-pure water. Not all samples contained alkali feldspars. Some whole rocks Sr analyses were performed on leached powders used for Nd, for comparisons (see text). All Nd were loaded on Re filaments and run as oxide over a period of 6 months during which the mean $^{143}Nd/^{144}Nd$ value of our Aldrich laboratory standard was 0.511415 ±8 (n = 17) and fully consistent with the long-term Aldrich mean of 0.511418 (Thirlwall, 1991a,b). All Sr were loaded on Re filaments between two layers of TaF_5. They are given relative to a $^{87}Sr/^{86}Sr$ value of 0.710248 for SRM987 with an external precision of 0.000011 (n = 26 over 6 months). $^{87}Sr/^{86}Sr$ ratios were corrected for initial values using a Rb/Sr of 0.55 on average (the Rb/Sr of alkali feldspar is in the range 0.1–1 according to published values of solid-liquid partition coefficients for Rb and Sr in alkali feldspar). WR, whole rock; AF, alkali feldspar.

Quartz and feldspar (samples E01–26 and EEW0043) minerals have been analysed for $\delta^{18}O$ using a VG Isotech (now VG instruments) Optimal dual inlet IRMS on line to the Laser Prep system (Mattey, 1997). Quantities of 1.7 mg for each hand-picked pure phase mineral have been combusted via a synrad CO_2 laser with presence of BrF_5 in excess. The released O_2 was directly analysed in the mass spectrometer, after cryogenic cleaned up. Three mineral standards were analysed during these runs: two are internal, GMG II, a garnet of +5.7 ‰ and a quartz of +8.8 ‰, which are calibrated against the international NBS-30 biotite at +5.1‰. All $\delta^{18}O$ are reported relative to V-SMOW. The overall precision on standards and sample replicates is better than ± 0.1‰.

compared with those of Gedemsa rhyolites thought to be generated by fractional crystallization of basaltic magma. It is apparent that the marginal rhyolites cannot be obtained by a single stage partial melting of basalts or their derivatives. The observed array of data is closely modelled by variable degrees of fractional crystallization of basalt.

Field observations show that the felsic rocks are always found in association with basalts and occur towards the upper part of an individual volcanic cycle, although there is a local recurrence of the basalt–rhyolite succession. This systematic stratigraphic relationship suggests that the silicic magmas are intimately associated with mafic magma, and the rhyolite marks the final phase of each magma intrusion cycle.

Crustal involvement on silicic magma through time

The focus of this study is to understand the compositional variation of the rhyolites through time, in an attempt to explain the role of rifting on the creation of large crustal magma reservoirs where mafic magma differentiate to give rise to silicic magmas. As observed in the MER, magma chambers occur where there is a dense network of faults, i.e. two or more trends of fault (Keranen *et al.* 2004).

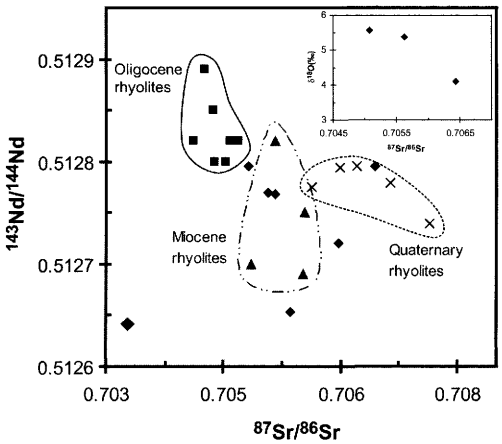

Fig. 3. Variation of $^{87}Sr/^{86}Sr$ vs. $^{143}Nd/^{144}Nd$ for rhyolites from the western margin of the Afar depression compared to the field of plateau and rift rhyolites. Note that most marginal rhyolites show substantial overlap with Miocene and Quaternary rhyolites. The inset displays variation of $^{87}Sr/^{86}Sr$ vs. $\delta^{18}O$ for rhyolites.

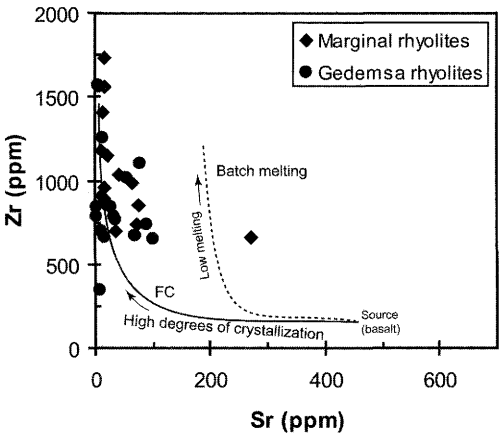

Fig. 4. Variation patterns of compatible (e.g. Sr) vs. incompatible (e.g. Zr) elements for west marginal rhyolites, illustrating that they can be modelled by fractional crystallization of basaltic magma. Also shown is the field of Gedemsa rhyolites thought to be generated by fractional crystallization of basaltic magma, and partial melting and fractional crystallization trends (calculated after Peccerillo *et al.* 2003).

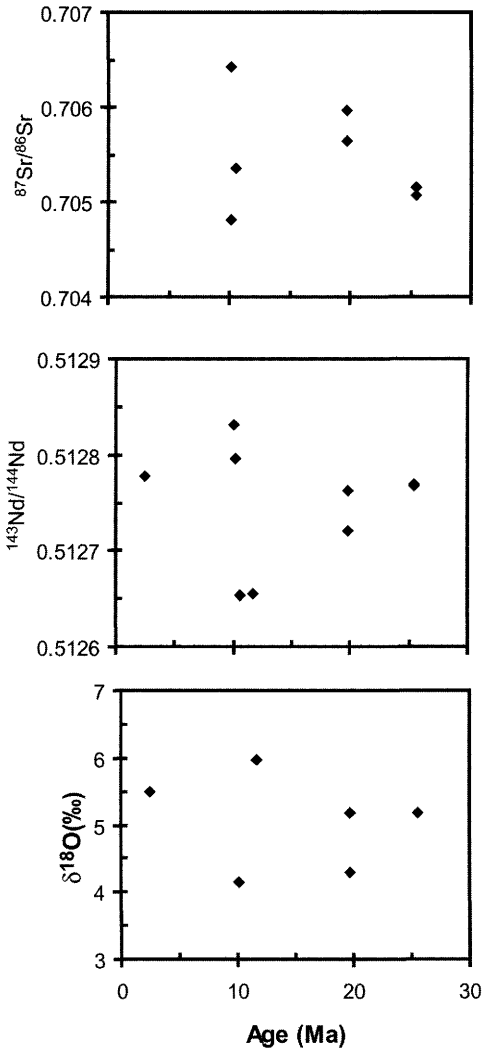

Fig. 5. Temporal variations of Sr, Nd and O isotope values for west marginal rhyolites. There is a trend between sample age and $^{87}Sr/^{86}Sr$, $^{143}Nd/^{144}Nd$ and $\delta^{18}O$.

In a plot of Sr–Nd–O isotope values with sample age (Fig. 5), there is a discernible trend. There is a negative correlation between sample age and $^{87}Sr/^{86}Sr$ values. $^{143}Nd/^{144}Nd$ ratios are roughly positively correlated with sample age. $\delta^{18}O$ decrease with time. There is no such systematic variation between major and trace elements, and sample age (not shown). The observed Sr–Nd–O isotope variations with time clearly reflect increasing participation of the basement over time on the genesis of silicic magma. This is most likely caused by progressive thermal and mechanical weakening of the crust within the faulted rift valley, and a concomitant shallowing in depth to the brittle–ductile transition in response to lithospheric thinning and magma injection in the past *c.* 30 Ma (Bastow *et al.* 2005; Stuart *et al.* 2006; Maguire *et al.* 2006).

The temporal variation of Sr–Nd–O isotopes of the western margin rhyolites indicates that the input of crust (or the rate of crustal contamination) on silicic magma generation is controlled by the stage of rifting and rate of magma addition. In the earliest stage (*c.* 30 Ma), the crust was unstretched and cold, and consequently the amount of assimilation of colder crustal rocks was limited. The repeated addition of large volumes of melt into the lithosphere during rifting would lead to weakening and heating of the crust, resulting in an increase in the rate of contamination.

^{18}O depletion in the marginal rhyolites suggests that meteoric fluids were involved in the magmatic process, under high temperature conditions. Crustal rocks have generally both $^{87}Sr/^{86}Sr$ and $\delta^{18}O$ high and hence crustal contamination will increase the $\delta^{18}O$, not deplete it, therefore fluid circulation must have occurred. Hence, contamination of the silicic magma must have occurred at shallow levels where hydrothermal fluids are normally found.

Conclusions

The timespan for silicic volcanism along the western margin of the southernmost sector of the southern Red Sea and the northernmost Main Ethiopian Rift indicates southward younging along the border fault and migrates from the wider border faults towards narrow (*c.* 10 km-wide) magmatic segments within the central rift. This indicates riftward migration of the locus of magmatism and faulting through time.

The felsic volcanic strata, capping the flood basalt sequences, are preferentially localized on or near the border fault, indicating that the age of the rhyolites actually dates the onset of rifting in the southern Red Sea and northern Main Ethiopian Rift. This clearly implies that rifting provides a mechanism for generation of large volumes of felsic magmatism.

The Sr–Nd–O isotopic data illustrate that the input of crust on the genesis of silicic magmas tends to increase with time, which suggests that the crust thermally weakens in response to lithospheric thinning and magma injection in the past ~30 Ma. The repeated addition of large volumes of melt into the lithosphere during rifting would lead to weakening and heating of the crust. Meteoric fluids were involved in the ^{18}O depletion of the marginal rhyolites.

Dereje Ayalew was supported by a travel grant from the Royal Society. Analyses were funded by the RHUL Research Committee. E. Bourdon was supported by EC Marie Curie Training and Mobility award. C. Ebinger and E. Wolfenden acknowledge support from University of London Research Funds, National Geographic Society, and NERC grant NER/A/S/2000/1004. A. Peccerillo and T. Furman are gratefully acknowledged for their insightful reviews.

References

ASRAT, A., BARBEY, P., LUDDEN, J.N., REISBERG, L., GLIEZES, G. & AYALEW, D. 2004. Petrology and isotope geochemistry of the Pan-African Negash pluton, northern Ethiopia: mafic–felsic magma interactions during the construction of shallow-level calc-alkaline plutons. *Journal of Petrology*, **45**, 1147–1179.

AYALEW, D. & YIRGU, Y. 2003. Crustal contribution to the genesis of Ethiopian plateau rhyolitic ignimbrites: basalt and rhyolite geochemical provinciality. *Journal of the Geological Society, London*, **160**, 47–56.

AYALEW, D., BARBEY, P., MARTY, B., REISBERG, L., YIRGU, G. & PIK, R. 2002. Source, genesis and timing of giant ignimbrite deposits associated with Ethiopian continental flood basalts. *Geochimica et Cosmochimica Acta*, **66**, 1429–1448.

BAKER, J., SNEE, L. & MENZIES, M. 1996. A brief Oligocene period of flood volcanism in Yemen: implications for the duration and rate of continental flood volcanism at the Afro-Arabian triple junction. *Earth and Planetary Science Letters*, **138**, 39–55.

BASTOW, I., STUART, G.W., KENDALL, J.M. & EBINGER, C. 2005. Upper mantle seismic structure in a region of incipient continental breakup: northern Ethiopian rift. *Geophysical Journal International*, **162**, 479–493.

CAMERON, K.L., PARKER, D.F. & SAMPSON, D.E. 1996. Testing crustal melting models for the origin of flood rhyolites: a Nd–Pb–Sr isotopic study of the Tertiary David Mountains volcanic field, west Texas. *Journal of Geophysical Research*, **101**, 20407–20422.

CHERNET, T., HART, W.K., ARONSON, J.L. & WALTER, R.C. 1998. New age constraints on the timing of volcanism and tectonism in the northern Main Ethiopian Rift–southern Afar transition zone (Ethiopia). *Journal of Volcanological and Geothermal Research*, **80**, 267–280.

COULIÉ, E., QUIDELLEUR, X., GILLOT, P.Y., COURTILLOT, V., LEFÈVRE, J.C. & CHIESA, S. 2003. Comparative K–Ar and Ar–Ar dating of Ethiopian and Yemenite Oligocene volcanism: implications for timing and duration of the Ethiopian traps. *Earth and Planetary Science Letters*, **206**, 477–492.

COURTILLOT, V., JAUPART, C., MANIGHETTI, I., TAPPONNIER, P. & BESSE, J. 1999. On causal links between flood basalts and continental breakup. *Earth and Planetary Science Letters*, **166**, 177–195.

CRISS, R.E. & TAYLOR, H.P. 1986. Meteoric–hydrothermal systems. *In*: VALLEY, J.W., TAYLOR, H.P. & O'NEIL, J.R. (eds) *Reviews in Mineralogy: Stable Isotopes in High Temperature Geological Processes*. Mineralogical Society of America, Vol. 16 Ch. 11, 373–424.

D'ACREMONT, E., LEROY, S., BESLIER, M.O., BELLAHSEN, N., FOURNIER, M., ROBIN, C., MAIA, M. & GENTE, P. 2005. Structure and evolution of the eastern Gulf of Aden conjugate margins from seismic reflection data. *Geophysical Journal International*, **160**, 869–890.

EBINGER, C.J. & SLEEP, N.H. 1998. Cenozoic magmatism throughtout east Africa resulting from the impact of a single plume. *Nature*, **395**, 788–791.

EBINGER, C.J., YEMANE, T., WOLDEGABRIEL, G., ARONSON, J.L., & WALTER, R.C. 1993. Late Eocene–Recent volcanism and rifting in the southern Main Ethiopian Rift. *Journal of the Geological Society, London*, **150**, 99–108.

EBINGER, C.J., YEMANE, T., HARDING, D., TESFAYE, S., REX, D. & KELLEY, S. 2000. Rift deflection, migration and propagation: linkage of the Ethiopian and Eastern rifts, Africa. *Geological Society of America Bulletin*, **102**, 163–176.

EILER, J.M. 2001. Oxygen isotope variations of basaltic lavas and upper mantle rocks. *In*: VALLEY, D.R. & COLE, D. (eds) *Reviews in Mineralogy: Stable Isotope Geochemistry*. Mineralogical Society of America, Vol. 43 Ch. 5, 319–364.

GEORGE, R., ROGERS, N. & KELLY, S. 1998. Earliest magmatism in Ethiopia: evidence for two mantle plumes in one flood basalt province. *Geology*, **26**, 923–926.

HALLIDAY, A.N., DAVIDSON, J.P., HILDRETH, W. & HOLDEN, P. 1991. Modelling the petrogenesis of high Rb/Sr silicic magmas. *Chemical Geology*, **92**, 107–114.

HANSON, G.N. 1989. An approach to trace element modeling using a simple igneous as an example. *In*: LIPIN, B.R. & MCKAY, G.A. (eds) *Reviews in Mineralogy: Geochemistry and mineralogy of the rare earth elements.* Mineralogical Society of America, Vol. 21, Ch. 4, 79–97.

HAWKESWORTH, C., KELLEY, S., TURNER, S., LE ROEX, A. & STOREY, B. 1999. Mantle processes during Gondwana break-up and dispersal. *Journal of African Earth Sciences*, **28**, 239–261.

HOFMANN, C., COURTILLOT, V., FÉRAUD, G., ROCHETTE, P., YIRGU, G., KETEFO, E. & PIK, R. 1997. Timing of the Ethiopian flood basalt event and implications for plume birth and global change. *Nature*, **389**, 838–841.

HUNEGNAW, A., SAGE, L. & GONNARD, R. 1998. Hydrocarbon potential of the intracratonic Ogaden basin SE Ethiopia. *Journal of Petroleum Geology*, **21**, 401–425.

KENDALL, J.M., STUART, G., EBINGER, C., BASTOW, I. & KEIR, D. 2005. Magma-assisted rifting in Ethiopia. *Nature*, **433**, 146–148.

KERANEN, K., KLEMPERER, S., GLOAGUEN, R. & EAGLE Working Group. 2004. Imaging a protoridge axis in the Main Ethiopian Rift. *Geology*, **39**, 949–952.

KIEFFER, B., ARNDT, N., *ET AL.* 2004. Flood and Shield basalts from Ethiopia: magmas from the African superswell. *Journal of Petrology*, **45**, 793–834.

MACKENZIE, G.D., THYBO, H. & MAGUIRE, P.K.H. 2005. Crustal velocity structure across the main Ethiopian Rift: results from two-dimensional wide-angle seismic modelling. *Geophysical Journal International*, **162**, 994–1006.

MARTY, B., PIK, R. & YIRGU, G. 1996. Helium isotopic variations in Ethiopian plume lavas: nature of magmatic sources and limit on lower mantle contribution. *Earth and Planetary Science Letters*, **144**, 223–237.

MATTEY, D.P. 1997. LaserPrep: An Automatic Laser-Fluorination System for Micromass 'Optima' or 'Prism' Mass Spectrometers. *Micromass Application Note*, **107**, 8pp.

MENZIES, M.A., KLEMPERER, S.L., EBINGER, C.J. & BAKER, J. 2002. Characteristics of volcanic rifted margins. *In*: MENZIES, M.A., KLEMPERER, S.L., EBINGER, C.J. & BAKER, J., (eds) *Volcanic Rifted Margins*, p. 1–14. *Geological Society of America Special Paper*, **362**.

PECCERILLO, A., BARBERIO, M.R., YIRGU, Y., AYALEW, D., BARBERI, M. & WU, T.W. 2003. Relationships between mafic and acid peralkaline magmatism in continental rift settings: a petrological, geochemical and isotopic study of the Gedemsa volcano, central Ethiopian rift. *Journal of Petrology*, **44**, 2003–2032.

PIK, R., DENIEL, C., COULON, C., YIRGU, G., HOFMANN, C. & AYALEW, D. 1998. The northwestern Ethiopian plateau flood basalts: classification and spatial distribution of magma types. *Journal of Volcanology and Geothermal Research*, **81**, 91–111.

PIK, R., DENIEL, C., COULON, C., YIRGU, G. & MARTY, B. 1999. Isotopic and trace element signatures of Ethiopian flood basalts: evidence for plume–lithosphere interactions. *Geochimica et Cosmochimica Acta*, **63**, 2263–2279.

ROCHETTE, P., TAMRAT, E., FÉRAUD, G., PIK, R., COURTILLOT, V., KETEFO, E., COULON, C., HOFMANN, C., VANDAMME, D. & YIRGU, G. 1998. Magnetostratigraphy and timing of the Oligocene Ethiopian traps. *Earth and Planetary Science Letters*, **164**, 497–510.

SCHILLING, J.G. & KINGSLEY, R.H. 1992. Nd–Sr–Pb isotopic variations along the Gulf of Aden: evidence for Afar mantle–plume–continental lithosphere interaction. *Journal of Geophysical Research*, **97**, 10,927–10,966.

TEKLAY, M., KRÖNER, A., MEZGER, K. & OBERHÄNSLI, R. 1998. Geochemistry, Pb–Pb single zircon ages and Rb–Sr isotope composition of Precambrian rocks from southern and eastern Ethiopia: implication for crustal evolution in east Africa. *Journal of African Earth Sciences*, **26**, 207–227.

THIRLWALL, M.F. 1991*a*. Long-term reproducibility of multicollector Sr and Nd isotope ratio analysis. *Chemical Geology*, **94**, 85–104.

THIRLWALL, M.F. 1991*b*. High-precision multicollector isotopic analysis of low levels of Nd as oxide. *Chemical Geology*, **94**, 13–22.

THIRLWALL, M.F., JENKINS, C., VROON, P.Z. & MATTEY, D. 1997. Crustal interaction during construction of ocean islands: Pb–Sr–Nd–O isotope geochemistry of the shield basalts of Gran Canaria, Canary Islands. *Chemical Geology*, **135**, 233–262.

UKSTINS, I., RENNE, P., WOLFENDEN, E., BAKER, J., AYALEW, D. & MENZIES, M. 2002. Matching conjugate volcanic rifted margins: $^{40}Ar/^{39}Ar$ chronostratigraphy of pre- and syn-rift bimodal flood volcanism in Ethiopia and Yemen. *Earth and Planetary Science Letters*, **198**, 289–306.

WATCHORN, F., NICHOLS, G. & BOSENCE, D. 1998. Rift-related sedimentation and stratigraphy, southern Yemen (Gulf of Aden). *In*: PURSER, B. & BOSENCE, D. (eds) *Sedimentary and Tectonic Evolution of Rift Basins*. Chapman & Hall, pp. 165–189.

WOLDEGABRIEL, G., ARONSON, J.L., & WALTER, R.C. 1990. Geology, geochronology and rift basin development in the central sector of the Main Ethiopian Rift. *Geological Society of America Bulletin*, **102**, 439–485.

WOLFENDEN, E., EBINGER, C., YIRGU, G., DEINO, A. & AYALEW, D. 2004. Evolution of the northern Main Ethiopian Rift: birth of a triple junction. *Earth and Planetary Science Letters*, **224**, 213–228.

WOLFENDEN, E., EBINGER, C., YIRGU, G., RENNE, P. & KELLEY, S.P. 2005. Evolution of the southern Red Sea rift: birth of a magmatic margin. *Geological Society of America Bulletin*, **117**, 846–864.